Meteorol. Atmos. Phys. 80, 117–129 (2002)

Meteorology and Atmospheric Physics

Department of Meteorology, University of Maryland, College Park, Maryland

Observed variations of leaf area index and its relationship with surface temperatures during warm seasons

M. Jin and **D.-L. Zhang**

With 9 Figures

Received October 13, 2001
Revised December 28, 2001

Summary

The leaf area index (LAI) is one of the most critical variables describing the biophysical and biochemical properties of the land cover in the remote sensing and climate models. In this study, the climatological variations of LAI is analyzed with NOAA's 14-year (1981–1994) Advanced Very High Resolution Radiometer (AVHRR) measurements. More attention is given to the 14 months of Julys or the warm seasons, in which interannual LAI variations contain more pronounced signals of dynamic forcing associated with the tropical rainforests and the temperate forests around 60° N. Furthermore, projecting the LAI anomalies into the empirical orthogonal function time series of El Niño and other climatologically important events shows that the large-scale circulations play an important role in determining the interannual variations of LAI, likely through the changes of surface insolation, precipitation and soil moisture. It is found that on the global scale LAI and the land surface and skin temperatures are negatively correlated, namely, decreasing LAI corresponds to warm temperatures. However, the regional LAI effects on the land surface climate vary significantly from regions to regions.

1. Introduction

Since the seminar work of Charney et al. (1977), it has been increasingly realized that biospheric variables could have an important impact on the regional and global climate. These variables often exhibit significant temporal (i.e., from the monthly, seasonal to annual time scales) and spatial variations. Most of such variations can be seen from the land surface temperatures. Furthermore, these variations and their impact on the land–biosphere–atmosphere system are more pronounced during the warm season than the cold season due to the presence of weak gradient large-scale dynamics but strong thermodynamics (Dickinson, 2001; Hurrell, 1996).

Specifically, the large-scale circulations can alter the land surface climate through changes in the soil moisture, surface insolation and temperature by propagating meteorological disturbances that are accompanied by clouds and precipitation, such as frontal systems, cyclones/anticyclones and tropical storms (van Loon and Rogers, 1978; Wallace and Gutzler, 1981; Barnston and Livezey, 1987). A good example is the recent winter warmth across Europe resulting from the low frequency variability of the North Atlantic Oscillation (NAO) (Hurrell, 1996; Thompson and Wallace, 2000). DeWeaver and Nigam (2000) reported the dynamical effects of NAO on the warming of Scandinavia and most of the cooling from the North Africa to the Caspian area. These large-scale effects are more significant in the middle to upper troposphere during the winter seasons.

In contrast, the local thermodynamics is closely associated with the heating/cooling and moistening/drying of the planetary boundary layer (PBL). That is, under the weak-gradient

large-scale environments, typically occurring in the tropics or during the summertime, the local thermodynamic conditions are more or less determined by the distribution and types of vegetation through the surface energy budget and water cycle, given the incoming solar radiation and topography (Zhang and Anthes, 1982). This is because vegetation can alter the surface albedo, roughness, the ability of transferring soil moisture into the air through evapotranspiration, and eventually the land near-surface air temperatures[1] (Ta) and skin temperatures[2] (Ts). Under favorable large-scale conditions, the PBL can provide sufficient sensible heat and ample moisture for the formation of clouds and precipitation. In fact, previous studies have shown close climatological relationships of the land surface temperatures and rainfall amount to the vegetation cover. For example, many land surface models showed that deforestation in the Amazonian tropics tends to decrease local precipitation, leading to an increase in surface temperatures (Zeng, 1999; Xue and Shukla, 1993; Xue et al., 1996; Pielke et al., 1997; Bonan et al., 1993).

An important recent finding shows that most of the local monthly climate variabilities over continents are caused by the land-surface processes (Koster and Suarez, 1995; Manabe and Stouffer, 1996). The influence of the large-scale dynamics appears to be more pronounced at the continental scale and beyond (e.g., the Pacific North American or PNA teleconnection), and over the time periods much longer than a month (e.g., the recent warmth across Europe).

To account for the land surface processes in climate models, various definitions of the Leaf Area Index (LAI) have been developed, based on satellite observations, to represent the physical and biophysical properties of vegetation (Sellers et al., 1996). LAI, mathematically defined as the area of one side of leaves per unit area, involves various physical and dynamical processes including the land surface radiative transfer, photosynthesis–conductance interactions, precipitation and interception at the canopy and surface (Sellers et al., 1996). In the context of radiative transfer, LAI represents the optical depth of a canopy. A vegetation canopy scatters incident solar photons largely by the orientation and structure of the leaves. In theory, this scattering is generally assumed to be isotropic. Therefore, the scattered radiation measured by a sensor above the canopy can be used to calculate LAI. In practice, however, LAI is derived from the Normalized Difference Vegetation Index (NDVI) after constraining the maximum and minimum NDVI values (Buermann et al., 2001; Los et al., 2000). The latter, related to the greenness and density of vegetation, is the difference of radiances between the Advanced Very High Resolution Radiometer (AVHRR) channels 1 and 2 divided by the sum of these two channels' radiances, i.e.,

$$\mathrm{NDVI} = \frac{R_{\mathrm{NIR}} - R_{\mathrm{VIS}}}{R_{\mathrm{NIR}} + R_{\mathrm{VIS}}}, \tag{1}$$

where R_{NIR} and R_{VIS} are the radiance from near-infrared and visible channels, respectively. NDVI, based on Eq. (1), is capable of detecting the vegetation photosynthetic activities (Justice et al., 1985; Tucker et al., 1991). However, NDVI can only be indirectly used through LAI to represent the vegetation effects in numerical models, namely

$$\mathrm{LAI} = \frac{\mathrm{NDVI}_{\mathrm{OBS}}}{\mathrm{NDVI}_{\mathrm{MAX}} - \mathrm{NDVI}_{\mathrm{MIN}}}\, x\mathrm{LAI}_{\mathrm{MAX}}, \tag{2}$$

where $\mathrm{NDVI}_{\mathrm{OBS}}$ is the observed NDVI from one pixel at a given time, $\mathrm{NDVI}_{\mathrm{MAX}}$ and $\mathrm{NDVI}_{\mathrm{MIN}}$ are the respective annual maximum and minimum values of NDVI for that pixel, and $\mathrm{LAI}_{\mathrm{MAX}}$ is the maximum LAI value for that pixel (Los et al., 2000). Similarly but independently, Myneni et al. (1996) calculated LAI from NDVI for a pre-specified biome through the curve fitting of LAI and NDVI (see their fig. 5). These studies demonstrated that LAI, evaluated from NDVI, could provide a reasonable description

[1]Ta, also called the screen-level air temperature, is the thermodynamic temperature measured by thermometers that are sheltered in a wooden box located at about 2 m above a flat grass land. It represents the combined effects of the air mass in the surface layer and the underlying land surface properties under the influence of the incoming solar and outgoing infrared radiation.

[2]Ts is the radiometric temperature derived from the thermal emission of the earth surface as some temperature average between various canopy and soil surfaces. Without any vegetation, Ts is the temperature of a molecular boundary or skin layer between soil and a turbulent air layer above. It can be inferred from the brightness temperatures after removing surface emissivity and atmospheric effects (Jin and Goetz, 2001). Thus, Ts represents the ground surface thermal conditions and is more determined by physical processes, such as latent and sensible heat fluxes (Jin and Dickinson, 2000; Jin et al., 1997).

of the fundamental properties of vegetation (Buermann et al., 2001).

The effects of LAI on the land surface climate may be understood from the physical law controlling the evolution of Ta and Ts, i.e., the energy conservation at the surface. That is, the net sensible (SH) and latent (LE) heat fluxes into a surface air layer must equal to the rate at which the thermal energy is stored (G), given the incoming solar radiation (Sn). Ts and Ta are important variables in such energy exchanges as shown by the following surface energy balance (SEB) equation,

$$\mathrm{Sn} + F_{\downarrow} - F_{\uparrow} + \mathrm{SH} + \mathrm{LE} = \mathrm{G}, \tag{3}$$

$$F_{\uparrow} = \varepsilon\sigma \mathrm{Ts}^4, \tag{4}$$

$$\mathrm{SH} = \rho\, \mathrm{C_p}\, \mathrm{C_H}\, \mathrm{U}\, (\mathrm{Ts} - \mathrm{Ta}), \tag{5}$$

$$\mathrm{LE} = \mathrm{L}\, \rho\, \mathrm{C_Q}\, \mathrm{U}\, (\mathrm{q_s}\, (\mathrm{Ts}) - \mathrm{q_a}), \tag{6}$$

where C_H and C_Q are the drag coefficients for sensible and latent heat fluxes, respectively; U is the surface wind speed, q_s is the saturation mixing ratio at Ts and all the other symbols assume their usual meteorological meaning. Although Ta and Ts are distinct in the physics definitions, they are consistent in terms of representing the interaction between the atmosphere and its underlying land cover. For this reason, the difference between Ta and Ts has been used to estimate the sensible and latent heat fluxes. For instance, Sun and Mahrt (1995) used Ts to replace the aerodynamic temperature in the conventional bulk equation to calculate the heat flux by including an extra roughness length into the drag coefficient. It follows that a better understanding of the relationship between LAI, Ta and Ts will shed light on the land–biosphere–atmosphere interactions and surface climate changes.

Most of the previous studies on the land–biosphere–atmosphere interactions were performed using the coupled atmosphere–land surface models involving the interactions of vegetation with the atmospheric temperature, precipitation, soil moisture and carbon dioxide (Deardorff, 1977; Charney, 1977; Dickinson, 1981; Keeling et al., 1996; Bounoua et al., 2000; Piekle et al., 2001). This vegetation or LAI mechanism was first suggested by Charney (1977) and subsequently studied by many others (e.g., Dickinson and Handerson-Sellers, 1988; Xue and Shukla, 1993; Xue et al., 1996; Pielke et al., 1997). Bonan (1997) showed an average 1 °C cooling over the eastern US and a warming over the western US during the summertime by varying vegetation types in his land-surface model. Significant dependence of the surface heat flux and temperature on LAI has also been reported by many other studies (e.g., Collins and Avissar, 1994; Li and Avissar, 1994; Bonan et al., 1993). In particular, Bonan et al. (1993) found that LAI is the most significant parameter accounting for the changes in the surface heat fluxes.

Although considerable advance has been made in understanding the vegetation effects on the land surface climate, they were mostly obtained from numerical modeling studies. Due to the lack of long-period data, few observational studies have been conducted to examine the geographical distribution and seasonality of LAI, and to assess its importance relative to the large-scale dynamics in determining the local surface climate change. Moreover, through the dynamical interactions, which are still poorly understood, the two different mechanisms may suppress or enhance each other's influences on the surface climate. In order to improve our capability of predicting the regional and global climate, it is highly desirable to investigate when and where the land cover may play an important role in the regional climate relative to the large-scale dynamics.

Therefore, the objectives of this study are to (i) examine the long-term global and regional variations of satellite-derived LAI and Ts and in situ measured Ta; and (ii) evaluate their relationships to the regional climate change. In addition, the National Centers for Environmental Prediction (NCEP) reanalysis will be used to help interpret the observed relationships among LAI, Ts and Ta. The next section describes briefly the data source used in this study. Section 3 presents the analyses of satellite-derived LAI and Ts and in situ measured Ta. A summary and conclusions are given in the final section.

2. Data sources

To achieve the above-mentioned objectives, we use the monthly LAI data and the monthly land skin temperature diurnal (LSTD) cycle data

during the period of 1981–1994 both at the horizontal resolution of 8 km. The former dataset was derived from AVHRR NDVI and provided by the remote sensing group at the University of Boston (Buermann et al., 2001), whereas the latter was based on NOAA-series AVHRR channels 4 and 5 thermal infrared observations and generated at the University of Maryland (Jin and Dickinson, 1999; 2000; 2001; Jin, 2000). To be compatible with the in situ air temperatures and the NCEP reanalysis, both datasets at the 8-km resolution are scaled up to 0.5 and 2.5 degree, respectively. A land-cover map (Hansen et al., 2001) originally obtained from AVHRR at the resolution of 0.00833 degree (about 1 km at equator) is aggregated to the current 0.0625 degree (about 8 km at equator), and now given at a latitude–longitude equal angle and in Goode's projection (Gleason, 1999).

Surface air temperatures were obtained from the conventional surface weather stations, after careful quality control as described in New et al. (1999). Problems or errors related to the raw measurements include the irregularity of shelters, changes of instruments, sparcity of observations over the arid and mountainous regions. These problems result often in some uncertainties in using the air temperature measurements. However, as New et al. (2000) estimated, monthly mean temperature anomalies at 0.5 degree have an accuracy of 0.5–1 °C. Thus, this dataset has widely been used in the previous global climate change studies (NRC 2000).

The National Center for Atmospheric Research (NCAR) and NCEP have conducted a 50-year (1948–1998) reanalysis of global meteorological observations at 2.5 degree resolution (Kietlet et al., 2001). This reanalysis includes observations at the land surface stations and ships, and from radiosondes, aircraft, satellites (e.g., HIRS) and other means. In this study, NCEP's reanalysis will be used to examine how the LAI changes are related to rainfall on the global scale.

3. Results

With the advances in remote sensing technologies, various land-cover properties can be detected by satellite-measured radiances (DeFries et al., 1998; Hansen et al., 2001). At present, several methods have been developed to infer the land cover properties all using the relationship between LAI and NDVI. Figure 1 shows the land cover information, used together with a look-up table, that was retrieved from NOAA's 8-km resolution AVHRR data. The land surface cover was categorized into thirteen vegetation classes, as given in Table 1, in which ocean and water surfaces are set to be class 0. It is apparent from Fig. 1a that tropical forests, the Saharan desert, the Boreal forests are well represented. To incorporate the above information into a land-surface model, a set of variables, such as LAI, can be designed for each class of the land cover to describe the surface properties, e.g., roughness length, water conductance, albedo, soil moisture and the other surface properties. For example, high albedo values may be assumed over the low- and mid-latitude desert areas and high-latitude snow areas, whereas large roughness lengths may be used for forest regions. A histogram of the global surface cover is given in Fig. 1b, which shows that land covers 26.2%, and ocean and lakes cover the rest of earth's surface. Among the 26.2% land cover, about 23.2% is bare soil (i.e., classes 12 and 13), 16.1% is grasses and crops (classes 10 and 11), 17.4% is shrubland (class 8), and 42.9% is forests and woodland (classes 1–7).

Figure 2 shows an example of the seasonal variations of LAI in the year of 1986, which just covers a natural life cycle of vegetation. No LAI values are assigned over desert areas (Fig. 2a–d), and over the higher latitudes during the cold season due to the snow coverage or the absence of greenness. The year of 1986 is chosen because it is a normal year in the context of global climate, namely, no El Niño-Southern Oscillation (ENSO) nor volcanic eruptions. Therefore, the monthly mean LAI of 1986 represents the typical climatology of the global land cover. Clearly, the land-cover distribution exhibits latitude and seasonal dependence mainly because the ecosystem requires appropriate temperatures and moisture at the surface and in soil; both are important variables associated with the land-surface climate. On the other hand, the ecosystem responds to the land-surface climate by modifying the land surface vegetation structures. Large seasonal variations and transitions of LAI between seasons are well observed in middle and higher latitudes

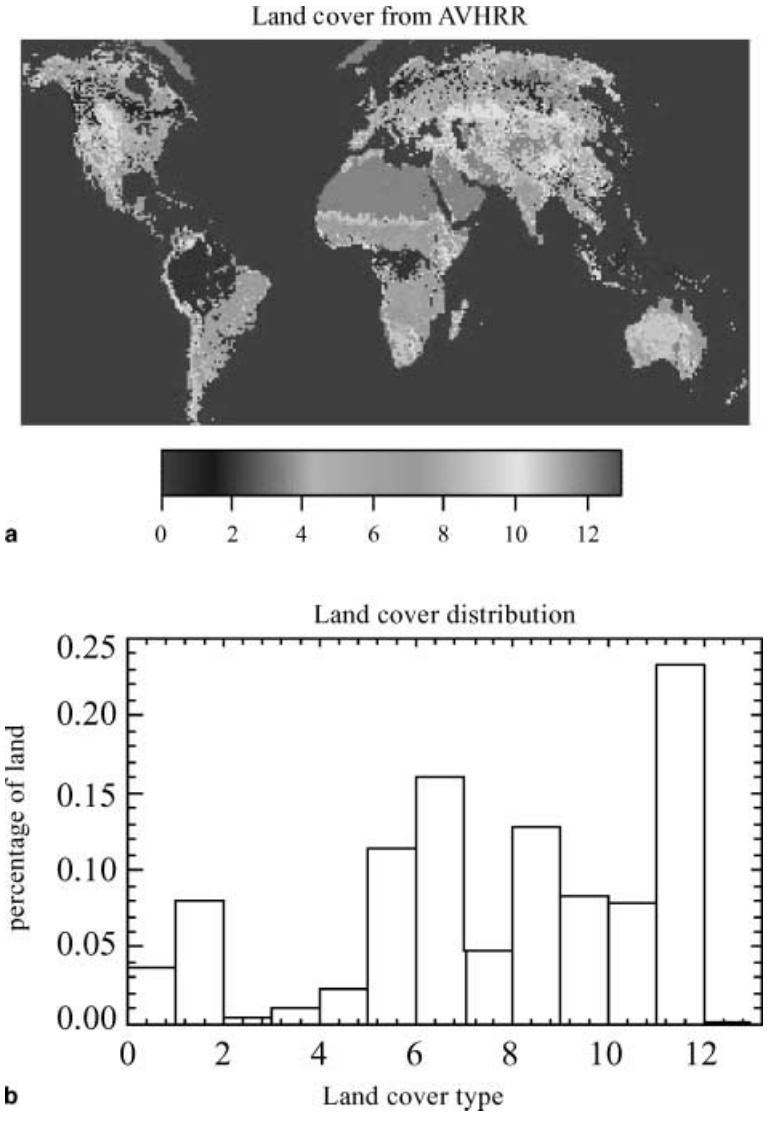

Fig. 1a. Global map of the land cover index averaged for the years of 1981–1994 from AVHRR; **b** Histogram of the percentage of each land cover class over the total land surface areas. Table 1 provides description of the land-cover index and corresponding vegetation types

with the most pronounced changes occurring between January and July. LAI increases during the growing season (Fig. 2b), reaches its peaks in the summer (Fig. 2c), and then gradually decreases as a result of losing greenness (cf. Fig. 2c and 2d). LAI for the temperate forests near 60° N has very high values (up to class 6) in July and no values in January. High LAI values are also associated with the tropical rainforests in July over the Amazon and southeast Asia. Over the United States, large LAI values are observed in the eastern half regions during the growing season (Fig. 2b). Since LAI is the optical depth of canopy that interrupts solar radiation reaching the surface, larger LAI values imply higher shortwave albedo and less radiative heating at the surface. Thus, the seasonal evolution of LAI would cause corresponding changes in the land surface temperatures. It should be pointed out, however, that the LAI values over the African rainforest regions are greater than expected in April and October (see Fig. 2b and 2d), implying some possible errors that may originate from either satellite observations or the retrieval process (Bounoua, 2001, personal communication).

In addition to the seasonal variations, LAI also varies significantly from year to year. To see this characteristic, the interannual variations of LAI for the years 1981–1994 are calculated as the LAI anomalies and then averaged globally. The results are given in Fig. 3a, which shows a slight decreasing trend of LAI from 1981–1994, though with some oscillations, except for the

Table 1. Description of land-cover index and vegetation types (from Hansen et al., 2001)

Land-cover index	Vegetation types
0	Water
1	Evergreen needle-leaf forest
2	Evergreen broad-leaf forest
3	Deciduous needle-leaf forest
4	Deciduous broadleaf forest
5	Mixed farming
6	Woodland
7	Wooded grassland
8	Closed shrubland
9	Open shrubland
10	Grassland
11	Cropland
12	Bare ground
13	Urban and built-up

large jumps in 1991 and 1994. The former jump may be attributed mainly to the volcanic eruption of Mt. Pinatubo in Philippine on 15 June 1991, and partly to the reduced accuracy of satellite retrieval associated with the volcano-generated aerosols. The LAI jump in 1994 appears to be caused by the satellite orbital drift in that year and a large volume of missing data over the Southern Hemisphere. If the two questionable years are removed, the decreasing trend of LAI suggests reduction of surface vegetation-related optical depth and an increase in the absorbed surface insolation, likely causing the global surface warming. This scenario is in general agreement with the warming trends seen in the Ts and Ta maps (Fig. 3b), which also exhibit oscillations similar to those of LAI (cf. Fig. 3a,b). Since Ts and Ta are related to LAI through several physical processes (e.g., the radiative transfer process at the surface, energy redistribution of sensible and latent heat, and photosynthesis–conductance processes), the high correlation between them demonstrates further the usefulness of LAI in parameterizing the effects of

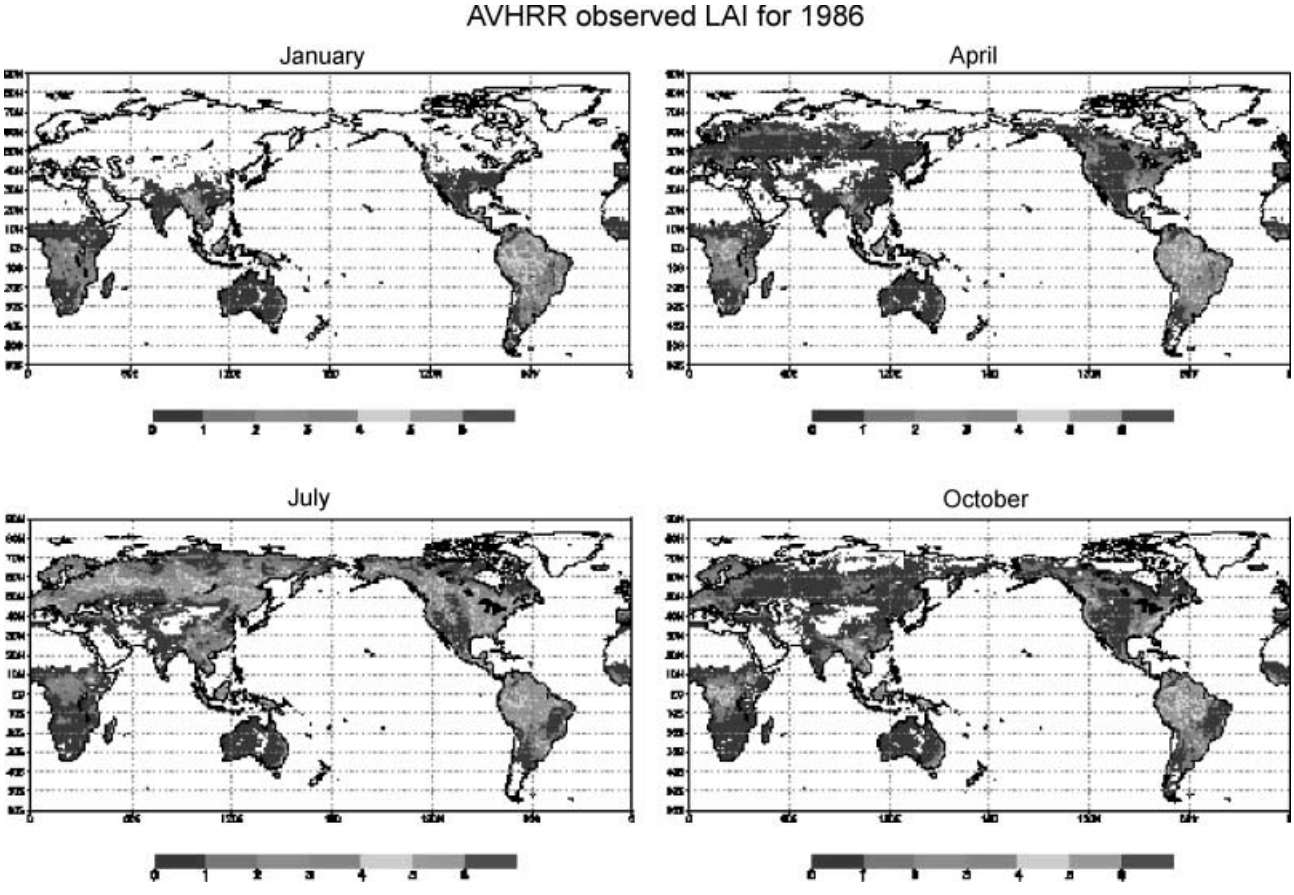

Fig. 2. Global distribution of the monthly averaged LAI from AVHRR for the month of **a** January, **b** April, **c** July, and **d** October of 1986

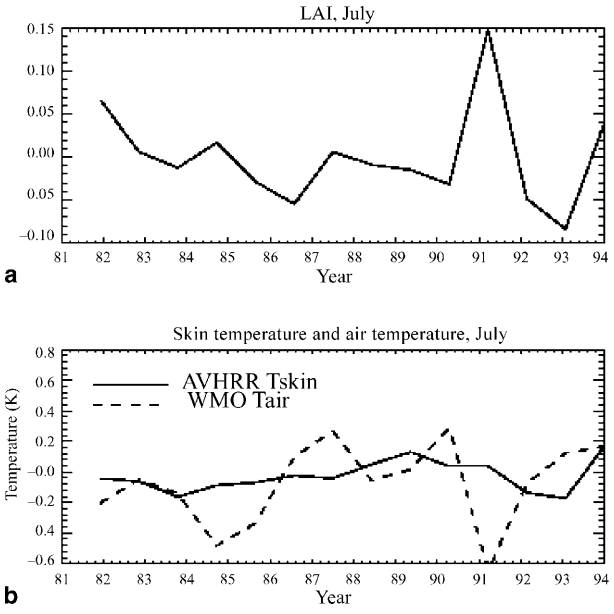

Fig. 3. Interannual variations of the globally averaged anomalies for **a** LAI; and **b** land skin and surface air temperatures during the years of 1981–1994. The LAI anomalies are obtained by the monthly average of only each July while the skin and surface temperatures are averaged for the months of January and July to represent the annual characteristics of these surface variables

vegetation on the land-surface climate. Moreover, although the Ts and Ta curves were obtained from different data sources, the interannual variations of their globally averaged anomalies are generally consistent with each other. A further understanding of the nonlinear relationship between Ts and Ta is one of the active research topics in the recent land surface studies, so it is beyond the scope of the present study.

While the interannual trends of globally averaged LAI are consistent with those of Ts and Ta, they are closely related to or affected by surface precipitation. For this purpose, Fig. 4 shows the global distribution of standard deviation of the LAI anomalies that are obtained after averaging 14 Julys during 1981–1994. The month of July is selected here because this month displays the largest LAI values over most areas globally (see Fig. 2). Peak LAI variations are evident for the tropical rainforests, temperate forests in both the Northern and Southern Hemispheres. The amplitude of the normalized LAI variations is as large as 0.9. Of importance is that the overall pattern of LAI standard deviation agrees well with the climatology of precipitation (cf. Figs. 4 and 5). For example, the large LAI variations over the 50–60° N belt coincide with significant amount of precipitation corresponding to the upward branch of Ferrel's circulation. Heavy rainfall also appears over the rainforest regions in Africa, the Amazon basin and southeast Asia where large LAI variations are present. In the

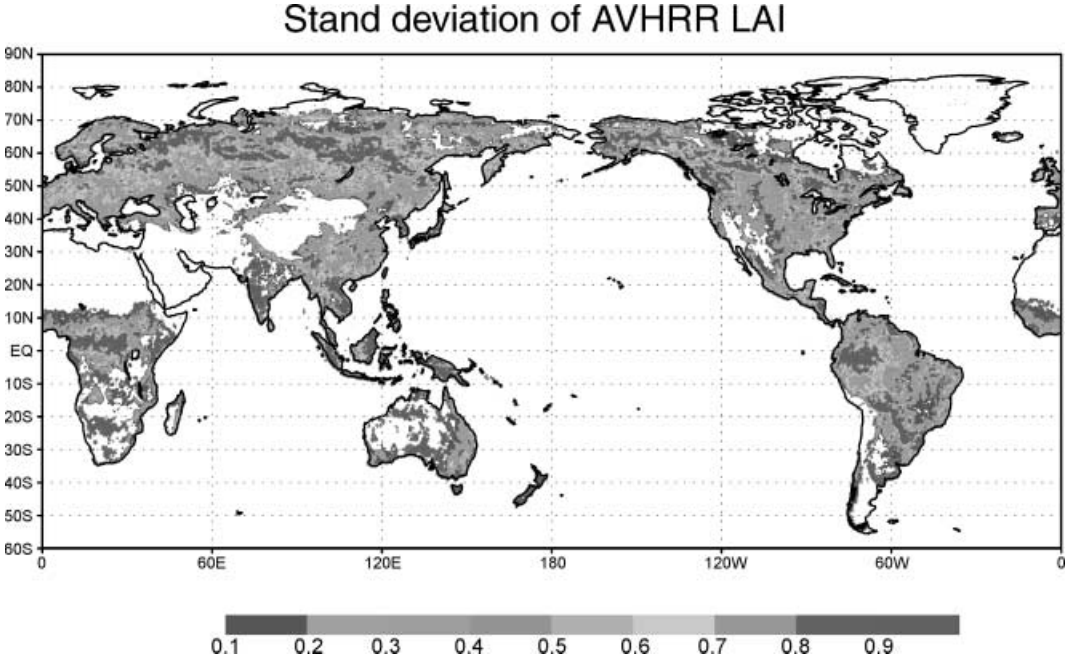

Fig. 4. Global distribution of the standard deviation of normalized LAI anomalies for the Julys of 1981–1994

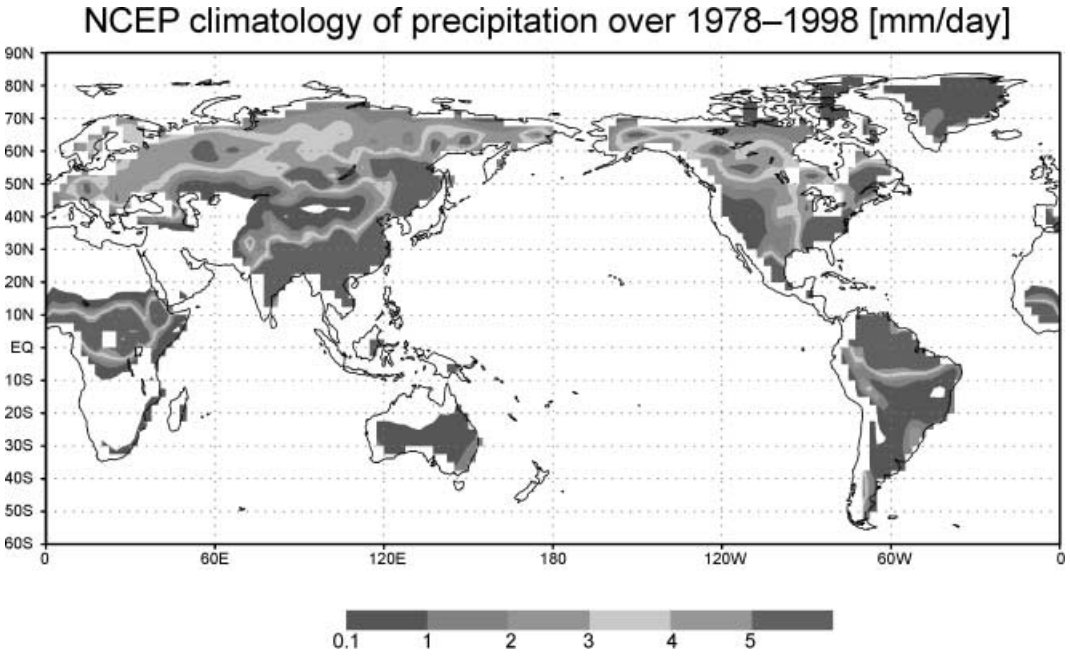

Fig. 5. Climatology of daily precipitation (mm) from NCEP's reanalysis for the years of 1979–1998

United States, the correlation between the precipitation amount and LAI variations is also very high; e.g., the wet eastern states exhibit large LAI changes. Thus, these results show clearly that the LAI or vegetation changes are closely related to the amount of rainfall. Despite the significant correlation, there are also areas of small precipitation with large LAI changes, such as over some portions of Australia where July is often dry with the average rainfall rates less than 1 mm/day, but the LAI changes are as high as 0.9.

As mentioned in Introduction, it is also desirable to gain insight into the LAI variations in response to the changes in the large-scale circulations. Thus, Fig. 6 shows the influence of El-Niño events on the LAI anomalies for the Julys of 1981–1994. Figure 6a is the time series of the leading mode of empirical orthogonal function (EOF) for equatorial Pacific sea-surface temperature (SST) anomalies over Niño-3 area (Mitchell and Wallace, 1998). There were 5 El-Niño events that occurred in this study period, as indicated by major peaks in the time series. Figure 6b shows the correlation coefficients between the Julys' LAI anomalies and the 5 El-Niño events in the years of 1981–1994. Large positive coefficients are observed over the United States, the central-eastern Africa and the northwestern Europe around the Black Sea. Median positive coefficients are noted over India and the central-eastern China. These patterns are in general agreement with the precipitation anomalies associated with ENSO (Dai et al., 1999). This implies that the vegetation cover in these regions was favorably influenced by the ENSO-related precipitation. However, large negative coefficients (above -0.7) are present at Spain, the western Asia, the central and southern Africa and elsewhere, indicating that the LAI pattern does not follow completely the El-Niño-induced precipitation (Dai et al., 1999). Thus, we may state that LAI, with its own natural cycle, responds to but is not completely controlled by the large-scale dynamics. Some of the above regions appear to be influenced by high topography or receive little influence from the ENSO-related circulations.

Similarly, Fig. 7 shows the influence of Pacific decadal climate oscillation (PDO) on the LAI anomalies for the Julys of 1981–1994. The PDO time series used here was derived as the leading EOF of monthly SST anomalies in the North Pacific Ocean, poleward of 20° N (Zhang et al., 1997; Mantua et al., 1997). LAI varies significantly with PDO along the 50–60° N belt, i.e., in the North America, Europe, and the eastern Asia. Positive coefficients are noted at the western Siberian Plain, southeastern Australia, eastern Brazil and some areas over Amazon and

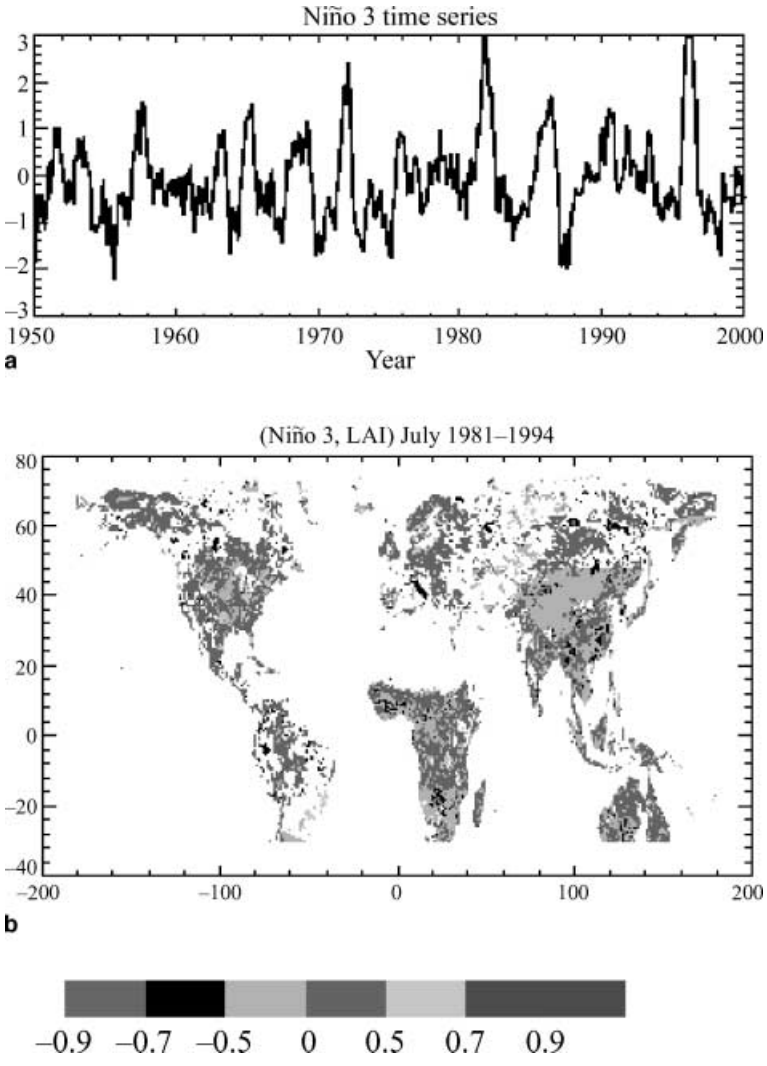

Fig. 6. The influence of El Niño on LAI: **a** the time series of Niño 3 in the past 50 years and **b** the correlation coefficients of LAI anomalies in Julys and Niño-3 time series for the years of 1981–1994

Africa. The correlation coefficients for PDO are generally higher than those for El-Niño and also cover relatively larger areas. This suggests that these regions are affected more by PDO than El-Niño, and that LAI may respond more strongly to the lower frequency oscillations in the large-scale dynamics. On the other hand, large areas in Asia and Africa exhibit negative correlations, indicating that the LAI variations may be determined by the processes, such as vegetation, topography and the other regional forcings.

We have also projected the LAI anomalies into the PNA and AO time series and noticed similar trends, namely, the influences of PNA and AO are significant over many regions around the globe (not shown). However, some areas still show little correlations with the large-scale flow anomalies, like those shown in Figs. 6 and 7. It follows that while a sizeable area of the global vegetation is significantly affected by the large-scale flows, there are exceptions for some regions where little correlation is present between the large-scale flow and local vegetation. This appears to depend critically on whether or not more precipitation will be produced under the influence of the large-scale forcing and local vegetation. Nevertheless, these large-scale signals are much less pronounced during the summer season than those during the cold season (not shown).

Since skin temperature is closely related to the land and biospheric interactions, Fig. 8 shows the correlation coefficients of LAI and Ts anomalies for the Julys of 1981–1994. Because of little vegetation over the desert areas, no coefficients are given in the North Africa, central Asia and part of Australia and South America. In general, the LAI and Ts anomalies are near-50% negatively and near-50% positively correlated around

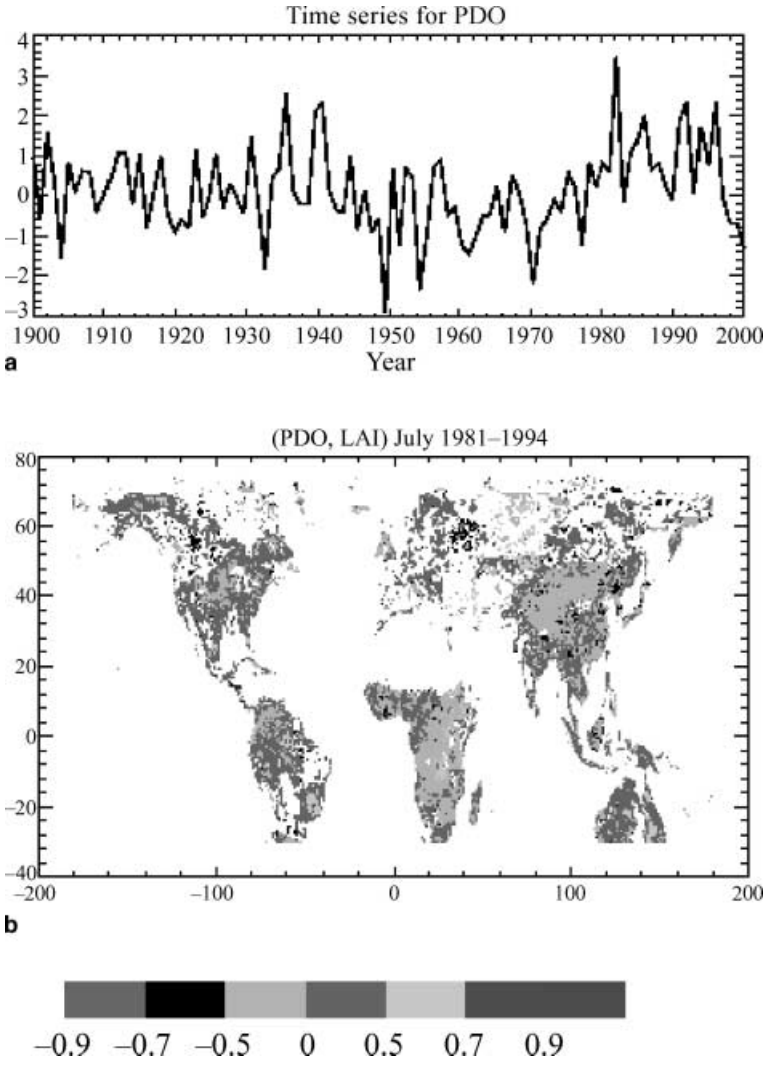

Fig. 7. The influence of the Pacific decadal climate oscillation (PDO) on LAI: **a** the time series of PDO in the past 100 years and **b** the correlation coefficient of LAI anomalies in Julys and PDO time series for the years of 1981–1994

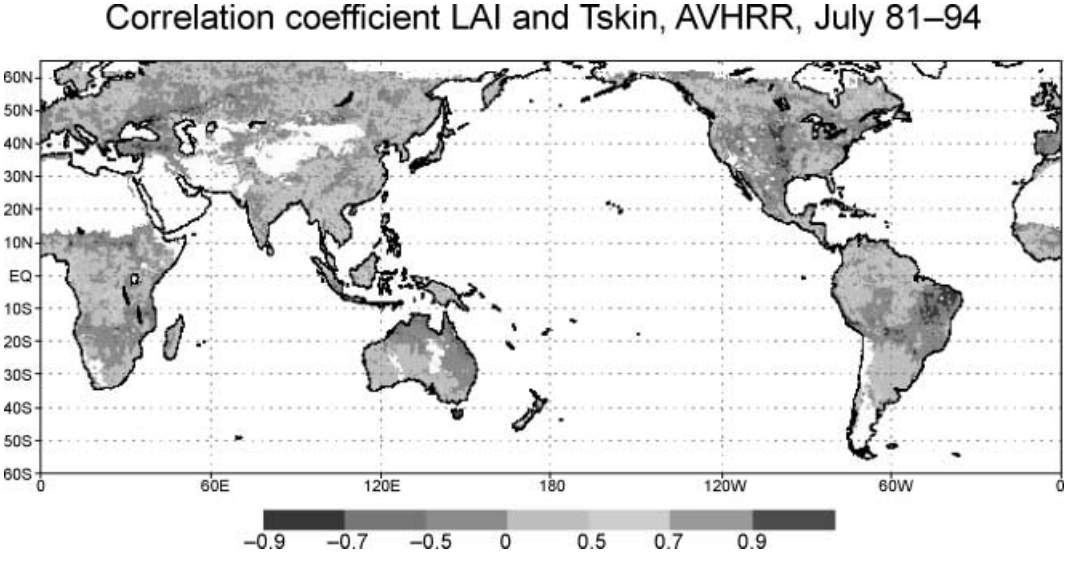

Fig. 8. Global distribution of the correlation coefficients between LAI and skin temperatures for the Julys of 1981–1994

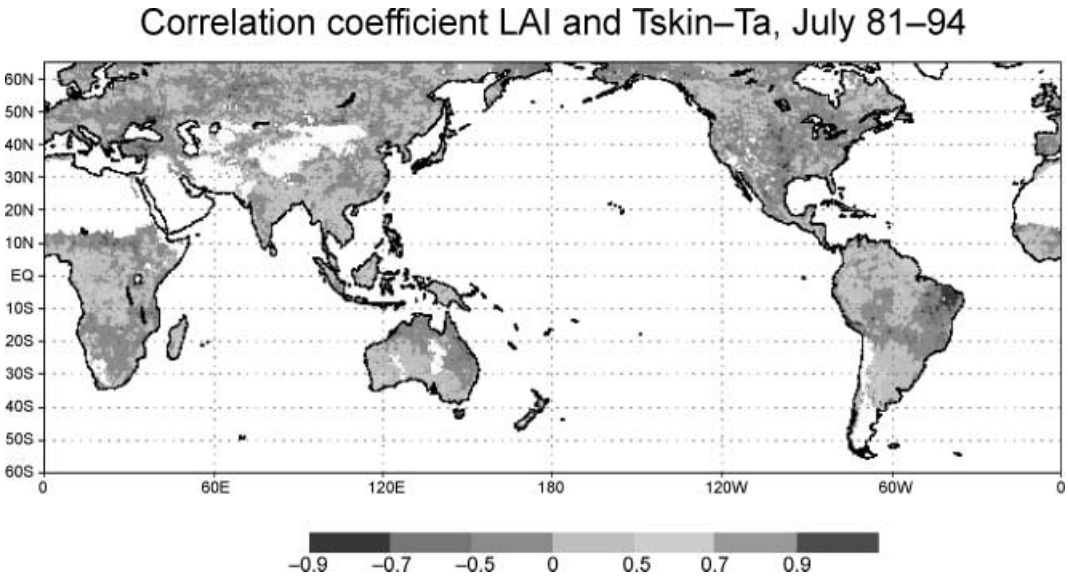

Fig. 9. Global distribution of the correlation coefficients between LAI and the differenced temperatures (i.e., Ts – Ta) for the Julys of 1981–1994

the globe, indicating the complicated feedback of LAI to the land surface climate. Specifically, large negative correlation is noted in the central United States and eastern Brazil where the atmosphere is relatively dry. By comparison, large positive coefficients are observed at the northwest coast of the Northern America, the northern portion of South America, the southern Asia and the central Africa, suggesting that the large-scale circulations appear to play an important role over these areas.

Finally, let us examine the correlation between the LAI and the difference of skin and surface temperatures (i.e., Ts – Ta) since the latter has been used to calculate the surface sensible heat flux. Figure 9 shows correlation patterns that are similar to those given in Fig. 8, suggesting that the LAI feedback has similar effects on the surface heat fluxes. That is, the vegetation growth or expansion, as a result of increased precipitation, tends to reduce the upward surface heat fluxes, and cool Ts and Ta. A comparison with the global precipitation pattern shows that the high coefficients regions (e.g., the central United States and the eastern Brazil) correspond to relatively dry environments. Over the wet areas, like the rainforests of Africa and northwestern North America, positive coefficients are observed. The results suggest that the LAI feedback to the surface heat flux is more important over relatively dry regions, whereas it is less significant over precipitation-rich areas than that of the large-scale dynamics.

4. Summary and conclusions

In this study, we examined the geographical distribution of LAI or the land cover and its importance in the land surface climate change using the 14-year (1981–1994) satellite observations. We have shown that a clear correlation between the decreasing LAI anomalies and the increasing Ts and Ta anomalies during the past two decades. More significant seasonal variations of LAI occur over the tropical rainforests, temperate forests, and the other areas where significant precipitation is observed.

However, there are pronounced spatial variations of the correlation between the LAI and the differenced temperature (i.e., Ts – Ta) anomalies around the globe. In most areas, the LAI changes correspond well to changes in Ts and Ta, whereas in the other areas LAI has little impact on the land surface climate. In the latter cases, precipitation and cloud amount appear to be the major parameters that determine the land surface changes.

By projecting the LAI variations into ENSO and PDO time series, we have shown that the large-scale circulations can have important

influences on LAI, Ts and Ta over many areas around the globe. However, the large-scale influence on these surface variables could not always be found. Thus, we may conclude that the land surface climate tends to be affected by both the large-scale circulations and the local LAI mechanism. During the warm seasons, the large-scale circulations tend to control the changes in vegetation through clouds and precipitation, while LAI helps determine the local surface climate through changes in surface insolation, soil moisture, evapotranspiration and roughness.

Acknowledgement

This work was partially supported by NASA's EOSIDS project and NOAA/GCIP's grant NA96GP0277. Dr. R. Dickinson is acknowledged for his support and guidance during the course of this study.

References

Barnston AG, Livesay RE (1987) Classification, seasonality and persistence of low frequency atmospheric circulation patterns. Mon Wea Rev 115: 1083–1126

Bonan GB (1997) Effects of land use on the climate of the United States. Climate Change 37: 449–486

Bonan GB, Pollard D, Thompson SL (1993) Influence of subgrid-scale heterogeneity in leaf area index, stomatal resistance, and soil moisture on grid-scale land–atmospheric interactions. J Clim 6: 1882–1897

Bounoua L, Coatz GJ, Los SO, Sellers PJ, Dazlich DA, Tucker CJ, Randall DA (2000) Sensitivity of climate to changes in NDVI. J Clim 13: 2277–2292

Buermann WJ, Dong X, Zeng N, Myneni RB, Dickinson RE (2001) Evaluation of the utility of satellite-based vegetation leaf area index data for climate simulations. J Clim 14: 3536–3551

Charney JG, Quirk WJ, Chow SH, Kornfield J (1977) A comparative study of the effects of albedo change on drought in semi-arid regions. J Atmos Sci 34: 1366–1385

Collins D, Avissar R (1994) An evaluation with the Fourier amplitude sensitivity test (FAST) of which land-surface parameters are of greatest importance for atmospheric modeling. J Clim 7: 681–703

Dai A, Trenberth KE, Karl TR (1999) Effects of clouds, soil moisture, precipitation, and water vapor on diurnal temperature range. J Clim 12: 2451–2437

Deardorff JW (1977) Efficient prediction of ground surface temperature and moisture with inclusion of a layer of vegetation. J Geophys Res 83: 1889–1903

DeFries RS, Hansen M, Townshend JRG, Sohlberg R (1998) Global land cover classifications at 8 km spatial resolution: The use of training data derived from Landsat imagery in decision tree classifiers. Int J Remote Sens 19: 3141–3168

DeWeaver E, Nigam S (2000) Zonal-eddy dynamics of the North Atlantic Oscillation. J Clim 13: 3893–3914

Dickinson RE (1983) Land surface processes and climate – surface albedo and energy balance. Adv in Geophys 25: 305–353

—, (2001) Interannual variability of climate – A review. Global Biogeochemical Cycles (in press)

Gleason ACR (1999) Effects of orbital drift on observations of land surface temperature recovered from the AVHRR sensors. M.S. thesis, The University of Maryland, 50 pp

Hansen MC, DeFries RS, Townshend JRG, Solberg R (2001) Global land cover classification at 1-km spatial resolution using a classification tree approach. Int J Remote Sens (in press)

Hurrell JW (1996) Influence of variations in extratropical winter warm teleconnections on Northern Hemisphere temperature. Geophys Res Letter 23: 665–668

Jin M (2000) Interpolation of surface radiation temperature measured from polar orbiting satellites to a diurnal cycle. Part 2: Cloudy-pixel treatment. J Geophys Res 105: 4061–4071

—, Dickinson RE (1999) Interpolation of surface radiation temperature measured from polar orbiting satellites to a diurnal cycle. Part 1: Without clouds. J Geophys Res 104: 2105–2116

—, Dickinson RE (2000) A generalized algorithm for retrieving cloudy sky skin temperature from satellite thermal infrared radiances. J Geophys Res 105: 27037–27047

—, Dickinson RE (2001) New evidence for global warming from satellite. Geophys Res Letter (in press)

—, Dickinson RE, Vogelmann AM (1997) A comparison of CCM2/BATS skin temperature and surface air temperature with satellite and surface observations. J Clim 10: 1505–1524

—, Goetz S (2001) A note on land surface temperature: Definitions, simulations, and application in land surface process models. J Geophys Res (accepted)

Justice CO, Townshend JRG, Holben BN, Tucker CJ (1985) Analysis of the phonology of global vegetation using meteorological satellite data. Int J Remote Sens 6: 1271–1318

Keeling CD, Chin JFS, Whorf TP (1996) Increased activity of northern vegetation inferred from atmospheric CO_2 measurements. Nature 382: 146–149

Koster RA, Suarez MJ (1995) Relative contributions of land and ocean processes to precipitation variability. J Geophys Res 100: 13,775–13,790

Li B, Avissar R (1994) The impact of variability of landscape characteristics on the variability of land-surface heat fluxes. J Clim 7: 527–537

Los SO, Collatz GJ, Sellers PJ, Malmstroem CM, Pollack NH, DeFries RS, Bounoua L, Parris MT, Tucker CJ, Dazlich DA (2000) A global 9-year biophysical land surface dataset from NOAA AVHRR data. J Hydrometeor 1: 183–199

Manabe S, Stouffer RJ (1996) Low-frequency variability of surface air temperature in a 1000-year integration of a coupled atmosphere–ocean–land surface model. J Clim 9: 376–393

Mantua NJ, Hare SR, Zhang Y, Wallace JM, Francis RC (1997) A Pacific interdecadal climate oscillation with impacts on salmon production. Bull Amer Meteor Soc 78: 1069–1079

Myneni RB, Nemani RR, Running SW (1997) Estimation of global leaf area index and absorbed par using radiative transfer models. IEEE Trans Geosci & Remote Sens 38: 1380–1393

New M, Hulme M, Jones P (1999) Representing twentieth-century space-time climate variability. Part I: Development of a 1961–90 mean monthly terrestrial climatology. J Clim 12: 829–856

—, Hulme M, Jones P (2000) Representing twentieth-century space-time climate variability. Part II: Development of 1901–1996 monthly grids of terrestrial surface climate. J Clim 13: 2217–2238

Pielke RA, Zeng X, Lee TJ, Dalu GA (1997) Mesoscale fluxes over heterogeneous flat landscapes for use in larger scale models. J Hydrology 1: 317–336

Sellers PJ (1987) Canopy reflectance, photosynthesis, and transpiration. II. The role of biophysics in the linearity of their interdependence. Remote Sens Environ 21: 143–183

—, Los SO, Tucker CJ, Justice CO, Dazlich DA, Collatz GJ, Randall DA (1996) A revised land surface parameterization (SiB2) for atmospheric GCMs. Part II: The generation of global fields of terrestrial biophysical parameters from satellite data. J Clim 9: 706–737

Sun J, Mahrt L (1994) Determination of surface fluxes from the surface radiative temperature. J Atmos Sci 52: 1096–1106

Thompson DWJ, Wallace JM, Hegerl GC (2000) Annular modes in the extratropical circulation. Part II: Trends. J Clim 13: 1018–1036

Tucker CJ, Dregne HE, Newcomb WW (1991) Expansion and contraction of the Saharan desert from 1980 to 1990. Science 253: 299–301

van Loon H, Rodgers JC (1978) The seasaw in winter temperatures between Greenland and Northern Europe. Part I: General description. Mon Wea Rev 106: 296–314

Wallace JW, With DS, Gutzler (1981) Teleconnections in the geopotential height field during the northern hemisphere winter season. Mon Wea Rev 109: 784–812

Xue Y, Shukla J (1993) The influence of land surface properties on Sahel climate. Part I: Desertification. J Clim 6: 2232–2245

Xue Y, Fennessy MJ, Sellers PJ (1996) Impact of vegetation properties on U.S. weather prediction. J Geophys Res 101: 7419–7430

Zeng N (1999) Seasonal cycle and interannual variability in the Amazon hydrologic cycle. J Geophys Res 104: 9097–9106

Zhang D, Anthes RA (1982) A high-resolution model of the planetary boundary layer – Sensitivity tests and comparisons with SESAME-79 data. J Appl Meteor 21: 1594–1609

Zhang Y, Wallace JM, Battisti DS (1997) ENSO-like interdecadal variability: 1900–93. J Clim 10: 1004–1020

Authors' address: Dr. Menglin Jin and Da-Lin Zhang, Department of Meteorology, University of Maryland, College Park, MD 20742-2425, USA (E-mail: mjin@atmos.umd.edu